Applied Thermal Engineering 121 (2017) 853–862

Contents lists available at ScienceDirect

Applied Thermal Engineering

journal homepage: www.elsevier.com/locate/apthermeng

Research Paper

Heat transfer performance of aviation kerosene RP-3 flowing in a vertical helical tube at supercritical pressure

Jie Wen [a], Haoran Huang [a], Yanchen Fu [a,*], Guoqiang Xu [a], Kun Zhu [b]

[a] National Key Laboratory of Science and Technology on Aero-Engine Aero-thermodynamics, Collaborative Innovation Center of Advanced Aero-Engine, School of Energy and Power Engineering, Beihang University, Beijing 100191, People's Republic of China
[b] AVIC Academy of Aeronautic Propulsion Technology, Beijing 103400, People's Republic of China

HIGHLIGHTS

- Buoyancy and centrifugal force effects exist in helical tube at supercritical pressure.
- Outside HTC is averagely 31.5% larger than the inside at the same cross section.
- Centrifugal secondary flow plays the key factor to cause heat transfer enhancement at the Richardson ratio $\varphi > 10$.
- Two correlations of Nusselt number are developed based on the experimental data.

ARTICLE INFO

Article history:
Received 18 February 2017
Revised 11 April 2017
Accepted 15 April 2017
Available online 20 April 2017

Keywords:
Heat transfer
Aviation kerosene
Vertical
Helical tube
Supercritical pressure

ABSTRACT

Convective heat transfer characteristics of aviation kerosene RP-3 at supercritical pressure (P = 5 MPa) in vertical helical tube were experimentally studied. The helical tube has 1.82 mm equivalent inner diameter, 20 mm helical diameter and 10 mm pitch. Circumferential temperatures were detected at both upward and downward flow experiments and the results indicated that: The secondary flow induced by centrifugal force moves outward of the cross section and inside temperature is larger than the outside. Thus, the outside heat transfer coefficient (HTC) is averagely 31.5% larger than that of the inside. Furthermore, heat transfer enhancement leading by centrifugal secondary flow is the key factor when the Richardson ratio is larger than 10. At last, two correlations of Nusselt number are developed to predict heat transfer of aviation kerosene RP-3 in helical tube based on experimental data at supercritical pressure.

1. Introduction

As one of typical curved tubes, helical tube is widely used in heat exchange equipment in power, petrochemical and air conditioning industries due to the advantages of easy processing and high surface volume ratio. The bending of helical tube could induce secondary flow along the tube axis, which leads to the different heat transfer performance compared with normal straight tube. Research on flow and heat transfer characteristics for regular fluid flowing in curved tubes have been done for decades. As one of the earliest researchers to study heat transfer in curved tubes, Dean proposed *De* number [1] to evaluate the level of flow centrifugal force. *De* number is defined as $Re\sqrt{\frac{d}{D}}$ and d, D represent tube diameter and helical diameter, respectively. Yang and Dong [2] numerically simulated convective heat transfer of fully developed laminar flow in helical tube and concluded the influences of *De* number, torsion and *Pr* number. The results show that the wall temperature gradient on one side could be enlarged due to the torsion effect and there is little effect on *Nu* number due to the low level of *Pr* number. Ebadian and his research group [3–5] systemically studied flow and heat transfer characteristics for regular fluid with constant properties flowing in curved tubes using numerical method. Their researches included various bending diameter and pitch, constant heat flux and wall temperature conditions. It is summarized that circular cross section temperature distribution is not symmetrical with the increase of pitch and the increase of *Pr* number will weaken the torsion effect on the heat transfer under laminar conditions. Moreover, the entrance effect could be ignored in curved tubes because the turbulent kinetic energy keeps at the high level. In order to verify the simulation results, mass of experiments about helical tube-shell heat exchanger were carried out. Ragbavan[6] carried out experiments to make comparison of

* Corresponding author.
E-mail address: yanchenfu@buaa.edu.cn (Y. Fu).

http://dx.doi.org/10.1016/j.applthermaleng.2017.04.055
1359-4311/

Nomenclature

A	surface area (m^2)
Bo^*	buoyancy number
C_p	isobaric specific heat capacity (kJ/(kg K))
d	diameter (m)
D	helical diameter (m)
g	gravitational acceleration (m/s^2)
G	mass flow rate ($kg/(m^2\ s)$)
Gr	Grashof number
h	heat transfer coefficient ($kW/(m^2\ K)$)
I	electrical current (A)
k	thermal conductivity (W/(m K))
L	length (m)
m	mass flux (g/s)
Nu	Nusselt number
n	coil numbers
P	pressure (MPa)
Pr	Prandtl number
Q	heat (W)
q	heat flux (kW/m^2)
$R(T)$	electronic resistivity (Ω m)
Ri	Richardson number
R	helical radius (m)
r	radius (m)
T	temperature (K)
Re	Reynolds number
U	voltage (V)

Greek

Φ	heat power (W)
δ	curvature
φ	Richardson ratio
ε	uncertainty
ρ	density (kg/m^3)
μ	dynamic viscosity (Pa s)
ν	kinetic viscosity (m^2/s)
λ	torsion

Subscripts

b	bulk
c	critical
f	film
in	inside
out	outside
pc	pseudo-critical
w	wall
x	local position

heat transfer coefficient (HTC) between helical tube and straight tube. The results mainly focused on temperature rise and found that HTC in helical tubes are 1.16 and 1.43 times larger than that in straight tubes under 40 °C and 50 °C conditions. The correlation of Nusselt number with relationships of *Re*, *Pr* and a/R is fitted in Coronel research [7] and HTC could be enhanced with the increase of helical curvature ratio. For many previous researches, heat transfer enhancement in turbulent flow in helical tube is not significant as that in laminar flow. Most of investigations like Mahajani [8], Janssen [9], Cengiz [10] and others [11–15] give a certain of correlations to evaluate heat transfer characteristics and those above are limited in specific working conditions.

In the application of aerospace thermal protection, compact heat exchange equipment could be widely used because of the CCA [16] technology. The hydrocarbon fuel flowing in the heat exchanger would be in the supercritical pressure. Thus, flow and heat transfer characteristics are vital important to be studied when the fluid is at supercritical status. Jackson and Hall [17–19] investigated mechanism of heat transfer deterioration and enhancement in different flowing directions. Experimental data and theoretical analysis indicated that radial temperature gradient would induce thermal property gradient, especially the density gradient, and then produce the effect of buoyancy lift. In addition, some dimensionless criterion numbers such as Bo^* and $Gr/Re^{2.7}$ were proposed to assess buoyancy influence on heat transfer. Furthermore, Jiang [20,21] and his group systemically studied local heat transfer variation for supercritical CO_2 flowing in micro-tubes with diameter of 0.27 mm, 1 mm and 2 mm. The results demonstrate that different phenomena of heat transfer enhancement and deterioration occur at different inlet temperatures. Also, buoyancy and thermal acceleration effects alternately occupy the key role to influence heat transfer at various working conditions. Compared with pure liquid, supercritical hydrocarbon fuel heat transfer are more complicated due to the component combination and chemical reactions at certain temperatures. Krieger [22] adopted SF6 to replace aviation kerosene and researched heat transfer variations with different physical factors at supercritical pressures. It is noted that the HTC keeps nearly the same for different flowing directions and system pressure has little effect when the inlet Reynolds numbers are higher than 20,000. Moreover, other researchers like Masters [23], Krasnoshchekov [24] and Benjamin [25] experimentally studied heat transfer characteristics of different supercritical hydrocarbon fuels and obtained some applicable *Nu* number correlations.

Investigations on flow and heat transfer of Chinese aviation kerosene RP-3 at supercritical pressures are widely conducted in the last decade. Thermal properties including critical point [26], isobaric specific heat capacity [27], density [28] and dynamic viscosity [29] were all obtained in our previous researches. Flow resistance and heat transfer characteristics [30–37] were studied when hydrocarbon fuel RP-3 flows in straight or U-turn micro-tubes. Considering the helical tube heat exchanger applied in the further CCA technology, heat transfer variation with helical effect at supercritical pressure would be more complicated and valuable to be studied. Hence, heat transfer performance of aviation kerosene RP-3 flowing in vertical helical tube at supercritical pressure is presented in this paper.

2. Test facility

2.1. Experimental system

The whole experiment was conducted in the experimental rig of flow and heat transfer on supercritical hydrocarbon fuel and the schematic is shown in Fig. 1. Hydrocarbon fuel from tank flowed through the fuel filter to remove impurities and then was pumped by a metering pump (SP6015, 15 MPa; 0.01–600 ml/min) to the main path. The fuel mass flux was measured by a Coriolis-force flow meter (Model: DMF-1-1, 0.15%, Sincerity). Two preheaters were set before the test section to heat the flowing fuel in order to achieve the required inlet temperature and the power is DC supply with 20 kW maximum capacity.

Two K-type armored thermocouples were inserted through joints to measure the inlet and outlet fuel temperatures. The hot

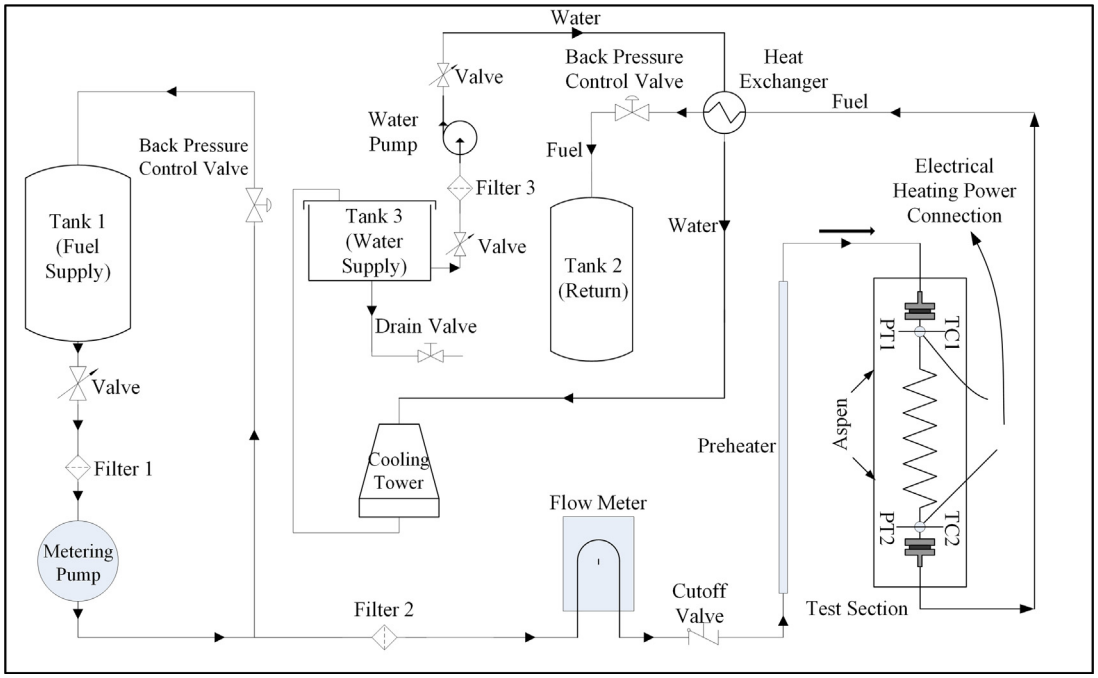

Fig. 1. Schematic of experimental system.

fuel was cooled down to room temperature by fuel-water heat exchanger and collected to the waste fuel tank after the measured system. One back valve and pressure gage transducer (Model 3051CA4, Rosemount) were connected to control and measure the static system pressure. Experimental data consist of absolute pressure, temperature, mass flow rate, heating voltage and current. All data were output in the form of electrical signals and gathered by ADAM-4018 data acquisition. Then it was transformed to several documents by ADAM-4520 and stored in the computer.

2.2. Test section

The experimental stainless steel tube has 1500 mm full length with 150 mm (L/d = 82.4) inlet and outlet developing sections. The helical tube diameter and pitch are fixed at 20 mm and 10 mm, respectively. All the experimental tube was processed into cylindrical right-lateral helical tube using standard abrasive tool. The helical tube inner diameter was measured by scanning electron microscope as shown in Fig. 2. The inner diameter varies from 1.72 mm to 1.85 mm and the hydraulic diameter was chosen to 1.82 mm as the same with straight tube.

NiCr-NiSi thermocouples are uniformly welded onto the outer wall of the whole helical tube as displayed in Fig. 3 with two flowing directions. Two thermocouples were set at the inside and outside of some same cross sections. In the later discussion, outside wall temperature would be used to analyze the variation if not specified. Table 1 shows the structure parameters of helical tube and all experimental conditions

2.3. Data reduction

The local HTC of helical tube is defined as follows:

$$h_x = \frac{q_x}{T_{wx,in} - T_{bx}} \tag{1}$$

where q_x is the effective heat flux and calculated by the difference between electrical power and heat losses.

$$q_x = \frac{I^2 R(T) / \left[\pi\left(d_{out}^2 - d_{in}^2\right)/4\right]}{\pi d} - q_{loss,x} \tag{2}$$

$q_{loss,x}$ represents the heat loss and its value is measured by the direct tube-heating before the hydrocarbon fuel experiments. The

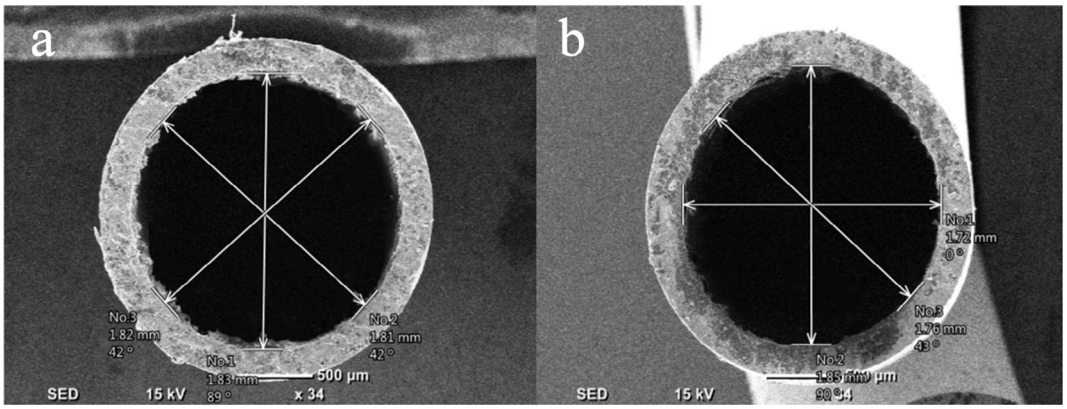

Fig. 2. SEM image of stainless steel tube (a: straight tube b: helical tube).

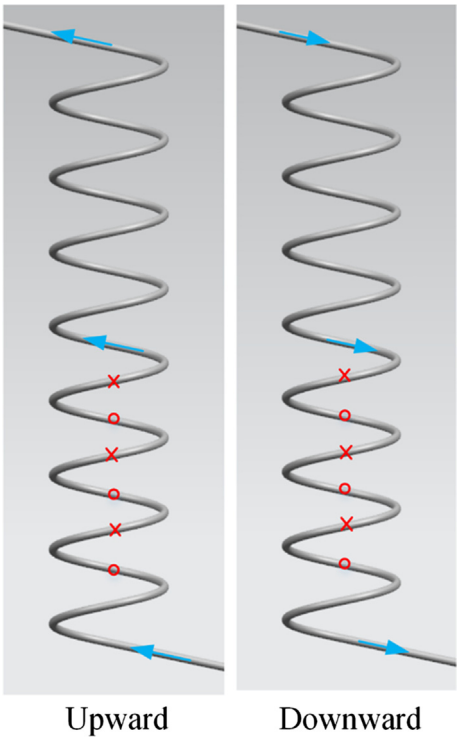

Fig. 3. Flow directions and thermocouple distribution in helical tube.

Table 1
Helical tube and experimental parameters.

Helical tube		Parameter	Range
Helical diameter (mm)	20	System pressure (MPa)	5
		Mass flux (kg/m^2 s)	534.5–1572
Pitch(mm)	10	Heat flux (kW/m^2)	37–596
Coil number	8	Inlet temperature (K)	323–633
		Flow direction	Upward and downward

temperature difference between tube wall and room temperatures, and heat loss power were obtained and their relationship was summarized by the nonlinear fitting method. $R(T)$ is electrical resistivity of the stainless steel tube. Local fuel temperature T_{bx} is determined by the relationships among the local heat flux, the inlet and outlet fuel enthalpy, which have been measured in previous research [38]. The following 1-D thermal conductivity equation is to calculate inner wall temperature at the cylindrical coordinate system.

$$\frac{\lambda}{r}\frac{\partial}{\partial r}\left(r\frac{\partial T}{\partial r}\right)+\dot{\Phi}=0 \tag{3}$$

The boundary conditions are

$$r=r_o,\quad \lambda\frac{\partial T}{\partial r}=q_{loss}(r) \tag{4}$$

Thus, $T_{wx,in}$ could be obtained by

$$T_{wx,in}=T_{wx,out}-\left[\left(\dot{\Phi}\frac{r_{out}^2}{2}-q_{x,loss}r_{out}\right)\ln\frac{r_{out}}{r_{in}}-\frac{\dot{\Phi}}{4}(r_{out}^2-r_{in}^2)\right]/k_x \tag{5}$$

$T_{wx,in}$ and $T_{wx,out}$ represent inner and outer wall temperatures of the experimental tube. $\dot{\Phi}$ is power produced by per unit volume of tube

Table 2
Experimental uncertainty of direct measurements.

Measured parameters	Instruments	Precisions
Mass flux	Coriolis force mass flow-meter	±0.15%
Outer wall temperature	K type thermocouple	±0.5 K
Fuel temperature	K type armored thermocouple	±0.5 K
Voltage	Voltmeter with output	±0.2%
Current	Ampere meter with output	±0.2%
Inner diameter	Scanning Electron Microscope	±0.0005 mm

resistance and k_x is local thermal conductivity of helical tube. Hence, the local Nusselt number is defined as follows:

$$Nu_x=\frac{h_x d}{\lambda_x} \tag{6}$$

where λ_x is local thermal conductivity of hydrocarbon fuel RP-3.

2.4. Uncertainty analysis

Table 2 shows the experimental uncertainty of direct measurements. As the total heat flux and heat loss are considered as two independent variables, the following uncertainty could be obtained based on error propagation formula:

$$\left|\frac{\Delta q_x}{q_x}\right|=\sqrt{\left(\frac{q_x+q_{loss}}{q_x}\right)^2\varepsilon^2(q_{0,x})+\left(\frac{q_{loss,x}}{q_x}\right)^2\varepsilon^2(q_{loss,x})} \tag{7}$$

Then the value is confirmed as 2.7% when the uncertainties of total heat flux and heat loss are calculated by the following formulas:

$$\left|\frac{\Delta q_{0,x}}{q_{0,x}}\right|=\sqrt{4\varepsilon^2(I)+\left(\frac{2d_{out}^2}{d_{out}^2-d_{in}^2}\right)^2\varepsilon^2(d_{\mathrm{out}})+\left(\frac{2d_{in}^2}{d_{out}^2-d_{in}^2}\right)^2\varepsilon^2(d_{in})+\varepsilon^2(d_{out})}=2.58\% \tag{8}$$

$$\left|\frac{\Delta q_{loss,x}}{q_{loss,x}}\right|=\sqrt{\varepsilon^2(I)+\varepsilon^2(U)+\varepsilon^2(d_{out})+\varepsilon^2(L)+\varepsilon^2(T_{wx,out})}=0.85\% \tag{9}$$

In all experimental conditions, the difference between inner and outer wall temperature is limited with 2 K and the uncertainty of the inner wall is 1.05 K. Also, the uncertainty of local fuel bulk temperature is 0.85 K according to the relationship between temperature and enthalpy. The temperature difference between inner wall and fuel bulk is higher than 30 K and the uncertainty could be defined.

$$\left|\frac{\delta(\Delta T)}{\Delta T}\right|=\frac{\sqrt{|\delta T_{wx,in}|^2+|\delta T_{bx}|^2}}{30}=4.5\% \tag{10}$$

Thus, the uncertainty of local HTC is calculated as

$$\left|\frac{\Delta h_x}{h_x}\right|=\sqrt{\varepsilon^2(q_x)+\varepsilon^2(\Delta T)}=\sqrt{(2.7\%)^2+(4.5\%)^2}=5.2\% \tag{11}$$

The thermal conductivity uncertainty of hydrocarbon fuel is within 3% according to the previous measurement results [39] and the uncertainty of inner diameter is 7.1%. Hence, the maximum uncertainty for Nusselt number could be defined as follows:

$$\left|\frac{\Delta Nu_x}{Nu_x}\right|=\sqrt{\varepsilon^2(h_x)+\varepsilon^2(\lambda)+\varepsilon^2(d_{in})}=\sqrt{(5.2\%)^2+(3.0\%)^2+(7.1\%)^2}=9.27\% \tag{12}$$

3. Results and discussion

3.1. Physical factors effect on heat transfer

Hydrocarbon fuel in helical tube is influenced by centrifugal force and then the secondary flow appears in the vertical direction to the main flow. Flow pattern in helical tube is mainly divided into laminar and turbulent flow like flow in a straight tube. The distinction between two kinds of flow pattern relies on the critical Reynolds number and three following formulas about critical Reynolds number obtained by Ito [40], Srinivasan [41] and Schmidt [42] are widely used to distinguish flow pattern.

$$\text{Ito}: Re_c = 2000\left(\frac{d}{D}\right)^{0.32} \tag{13}$$

$$\text{Srinivasan}: Re_c = 2100\left[1 + 12\left(\frac{d}{D}\right)^{0.50}\right] \tag{14}$$

$$\text{Schmidt}: Re_c = 2300\left[1 + 8.6\left(\frac{d}{D}\right)^{0.45}\right] \tag{15}$$

According to the structure of experimental helical tube, predictions of critical Reynolds number in three formulas are 7414, 7445 and 7199. Thus, the average value of 7350 is considered as the real critical Reynolds number in this research.

3.1.1. Effect of heat flux

Fig. 4 shows the bulk fuel temperature, inner wall temperature and Nusselt number variations for different heat fluxes when the inlet Reynolds number is 1360 in helical tube. It is seen that the inner wall temperature presents the rising tendency along the flow direction. The boundary layer thickness is larger to make poor heat transfer characteristics and the inner wall temperature is relative high at the entrance section. For the 60 kW/m^2 heat flux condition, the whole tube Reynolds number is lower than 7350 and flow pattern is laminar as seen in Fig. 4c. Thus, the Nusselt number is about 20 and much lower than that of other heat flux conditions. The other reason is that the isobaric specific heat capacity increases slowly when the film temperature is lower than pseudo-critical temperature. With the increase of heat flux, the flow pattern in helical tube turns to be turbulent and centrifugal force starts to enhance the flow mixing between the near wall and tube center. The HTC approximately increases with the linear tendency to twice larger than laminar state due to the dramatic increase of turbulence kinetic energy. In addition, Nusselt number increases in the exponential form at the high heat flux when the inner wall temperature is larger than the pseudo-critical temperature 716 K.

The HTC variation, inside and outside inner wall temperature distributions when the inlet Reynolds number is 3210 are displayed in Fig. 5. The results show that the inside wall temperature is always higher than the outside at the same cross section and the outside has the larger local HTC. It is explained that centrifugal force leads the main factor to affect circumferential wall temperature distribution. When the fuel flows through the helical tube, direction of centrifugal force with value u^2/r always points to the outside and secondary flow flows to the outside wall. The secondary fluid impingement would enhance the heat transfer and the outside HTC is averagely 31.5% larger than the inside. At the entrance region of dimensionless position x/d < 120, the inside wall temperature is higher than the outside due to the thicker boundary layer on the outside. The temperature gradient is relatively small and HTC along with helical tube increases slowly. After the inner wall temperature is beyond the pseudo-critical temperature, buoyancy effect becomes more significant to shift the temperature distribution at the cross section, and Fig. 5b shows that the local HTC values for both inside and outside are approaching.

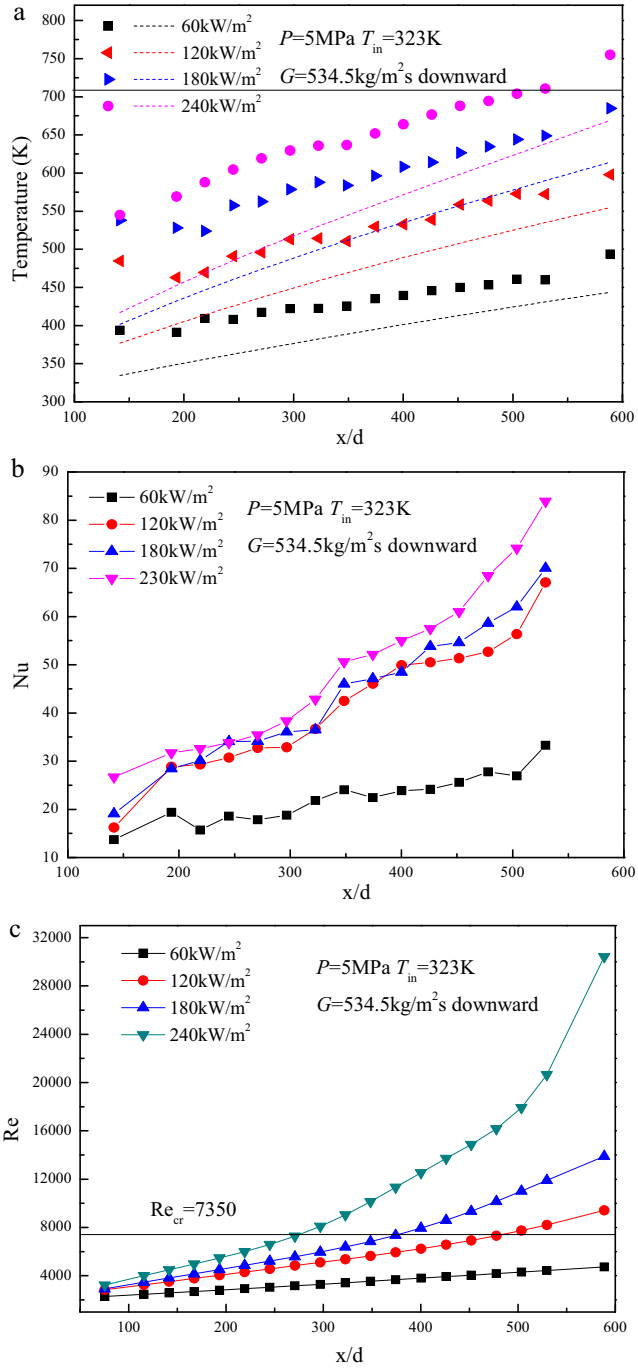

Fig. 4. Effect of heat flux on heat transfer at low inlet Reynolds number.

To evaluate the inlet Reynolds number influence on heat transfer, the flourishing turbulent for upward flow experiments were conducted as shown in Fig. 6. The inlet Reynolds number is 16,300 and heat flux varies from 120 kW/m^2 to 600 kW/m^2. It is demonstrated that there is no abnormal distribution points like peak or trough and the wall temperature uniformly increases. Besides, Nusselt number increases with the heat flux increasing because the turbulent kinetic energy induced by centrifugal force plays the key factor. At the condition of 600 kW/m^2, heat transfer is enhanced by the increase of isobaric specific heat capacity and decrease of dynamic viscosity. Fig. 6c displays the Bo* variation

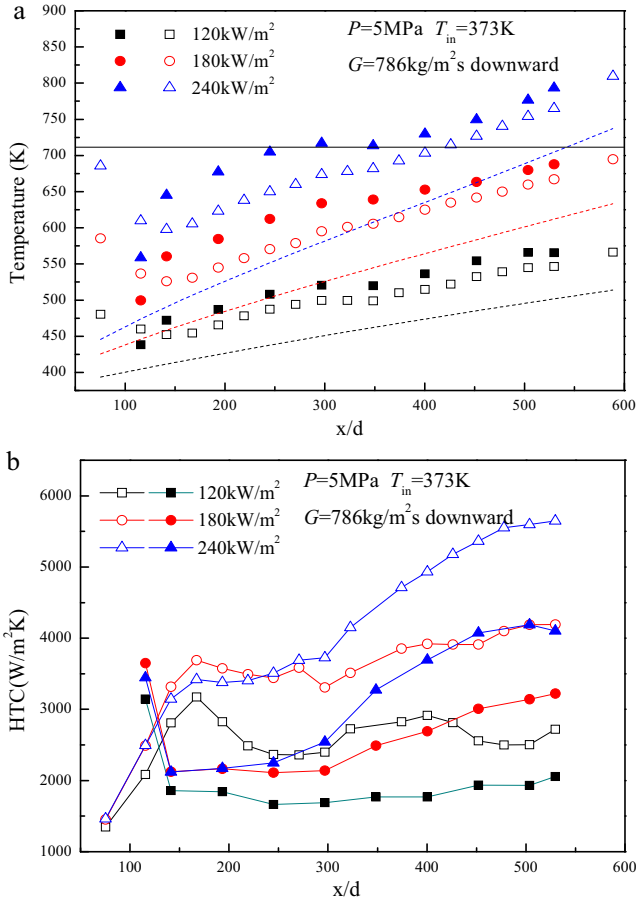

Fig. 5. Inside and outside heat transfer distribution at different heat fluxes.

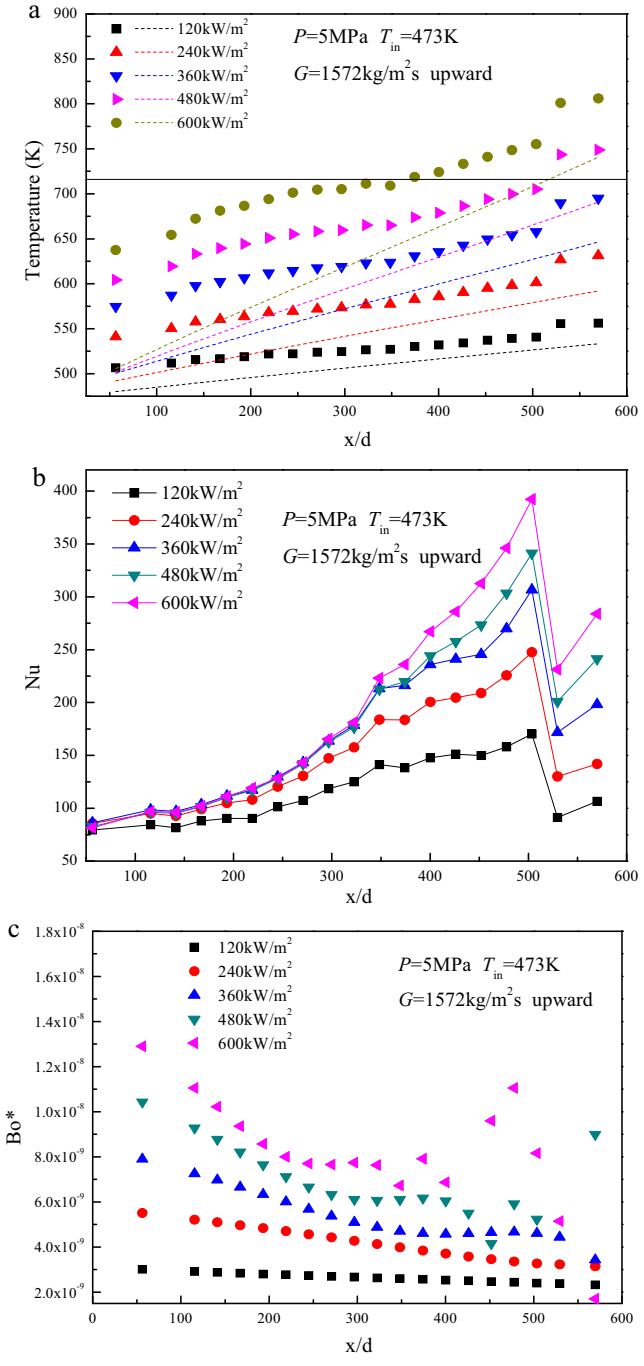

Fig. 6. Effect of heat flux on heat transfer at high inlet Reynolds number.

for the same condition that the maximum value is still far less than the buoyancy lift criterion $Bo^* < 2 \times 10^{-7}$ for supercritical hydrocarbon fuel in Jiang's [43] research. Even though there appears peak at the pseudo-critical region, secondary flow effect on heat transfer enhancement could cover the buoyancy lift.

3.1.2. Effect of mass flux

Mass flux variation could change heat transfer characteristics due to the level of centrifugal force in the mainstream flow. Fig. 7 shows the wall temperature, bulk fuel temperature and Nusselt number variations along with dimensionless position and local Reynolds number. It is demonstrated that the inner wall temperature sharply decreases with the decrease of boundary layer at the inlet region of laminar flow. Then the flow pattern develops to the turbulent with the uniform increase of wall temperature. There is no obvious peak observed along the whole helical tube. Furthermore, Reynolds number variation of lower mass flux has steeper increasing tendency at the position x/d > 450 due to the higher wall temperature and sharp density variation. Fig. 7b indicates that Nusselt number could improve with the increase of mass flux at the same dimensionless position. The large turbulent kinetic energy and uniform centrifugal force lead to the tiny temperature gradient difference near the inner wall. Hence, the local Nusselt number steadily increases along the helical tube.

To detect the buoyancy effect on heat transfer characteristics, Bo^* distribution at different heat fluxes is shown in Fig. 7c. Only when the mass flux is 534.5 kg/m^2 s, there exists situation that $Bo^* > 2 \times 10^{-7}$ at the inlet laminar flow region. Nevertheless, Nusselt number variation does not show significant enhancement or deterioration and the buoyancy effect is not obvious. It is explained that the secondary flow vertical to the mainstream flow could destroy the laminar boundary layer and restrain the development of temperature gradient. Thus, the Bo^* criteria of buoyancy could not be applied to laminar flow in the helical tube.

3.1.3. Effect of flow direction

Fig. 8 shows the inner wall temperature and local HTC variations for upward and downward flow under same working conditions. It is seen that wall temperature along the whole helical tube for upward flow is overall higher than the downward flow. The maximum temperature difference is about 30 K, which is considerable for a circular tube with 1.82 mm inner diameter. Two main

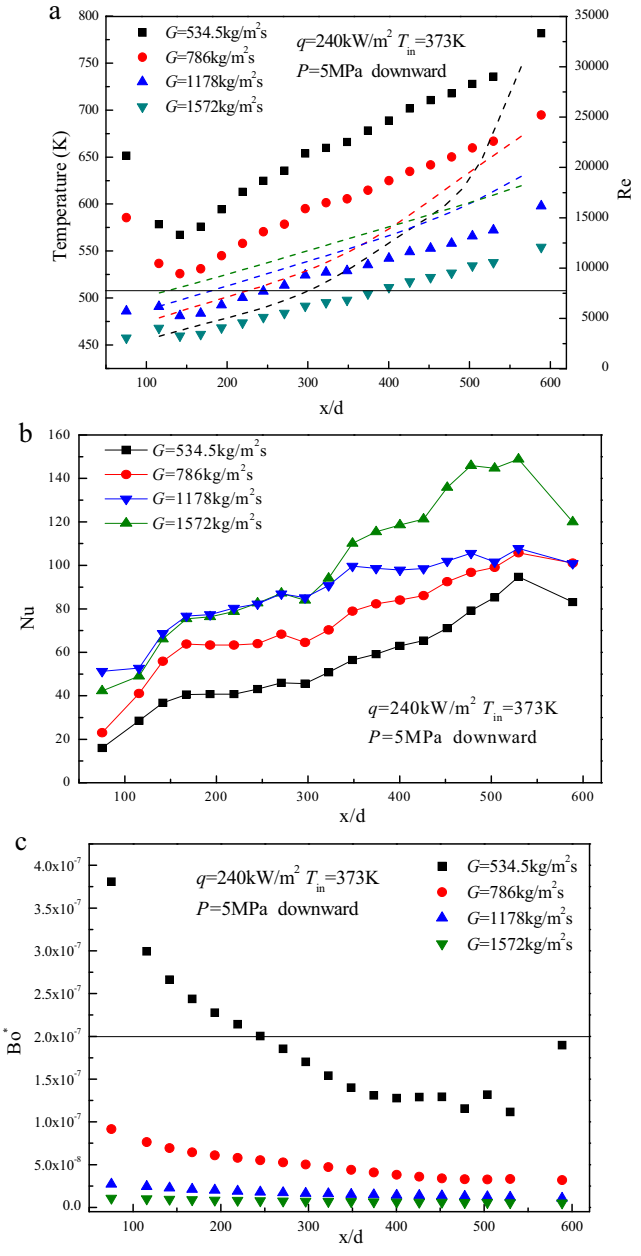

Fig. 7. Effect of mass flux on heat transfer in helical tube.

different heat transfer variation zones are divided by the dimensionless position x/d = 350. When the position is x/d < 350, the inner wall temperature rises across the region to critical temperature. The isobaric specific heat capacity peak appears to strengthen the convective heat transfer of downward flow and wall temperature rise slows down. However, buoyancy effect inhibits the increase of turbulent kinetic energy for the upward flow to make the wall temperature significantly higher than the downward flow. At the region of x/d > 350, buoyancy could influence the magnitude of radial centrifugal force and restrain the ability of heat transfer enhancement. Thus, inner wall temperatures come closer and HTC stays at the same level for both upward and downward flows.

Hydrocarbon fuel flowing in the vertical helical tube is mainly motivated by inertia force, buoyancy and centrifugal force as shown in Fig. 9. As the experimental tube is dextrorotation helical tube and directions between centrifugal force and vertical are obtuse angle. Then the buoyancy operation has remarkable decline

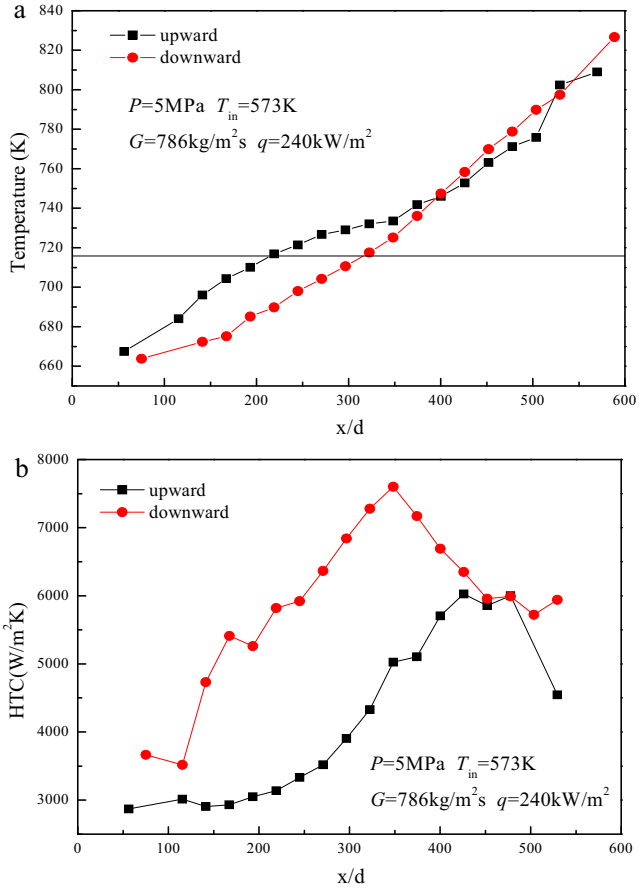

Fig. 8. Inner wall temperature and HTC distributions for upward and downward flows.

effect in the direction of centrifugal force when the flow direction is downward. The combined effect reduces the velocity gradient in the axial position and heat transfer enhancement is restrained. Moreover, the phenomenon that HTC decrease at the latter of helical tube for the upward flow could be explained by the above reason. With the increase of heat flux, the inner wall temperature is approaching the pseudo-critical temperature at the 5 MPa system pressure. Thermal properties such as isobaric heat capacity, density and dynamic viscosity sharply changes, which leads to the significant HTC peak at the middle of the dimensionless position.

3.2. Combined effect of properties variation and centrifugal force

Hydrocarbon fuel flowing in the helical tube could product secondary flow and make the HTC higher than that in the straight tube under same conditions. There exist three kinds of secondary flow in the helical flow: Dean Vortex [1] in the main stream flow, Morton vortex [44] induced by buoyancy secondary flow vertical to the main flow and Wang vortex [45] induced by torsion. As the intensity of Wang vortex is defined as

$$u_{Gn}/u_{ax} = \frac{2\pi\lambda\delta}{1+4\pi^2\lambda^2} \tag{16}$$

where λ is torsion defined by $\lambda = \frac{p}{\pi D}$ and δ is curvature defined by $\delta = \frac{d}{D}$. According to the experimental tube parameter, the intensity value of torsion vortex is about 0.0455 and the secondary flow influence induced by torsion could be neglected in this research.

For heat transfer analysis flowing in the vertical straight tube, Jackson [17] proposed $Gr/Re^{2.7}$ to evaluate the buoyancy effect at

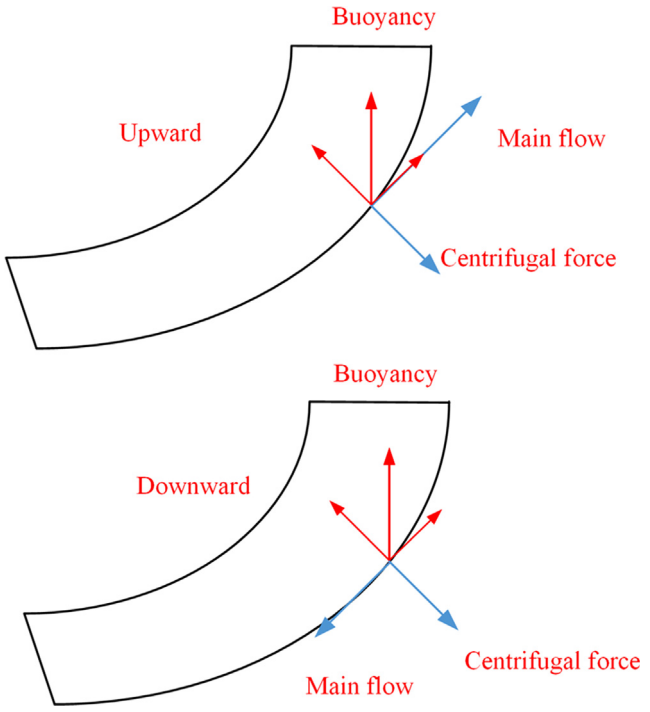

Fig. 9. Stress diagram for aviation kerosene RP-3 in helical tube.

the critical zone. Considering the helical tube with large curvature and small helical diameter, Ciofalo [46] used the following equation to define gravitational and centrifugal Richardson numbers.

$$Ri_g = \frac{Gr_g}{Re_b^2} \tag{17}$$

$$Ri_c = \frac{Gr_c}{Re_b^2} \tag{18}$$

where gravitational and centrifugal Grashof numbers are defined as follows:

$$Gr_g = \frac{(\rho_w - \rho_b)\rho_b g d^3}{\mu_b^2} \tag{19}$$

$$Gr_c = \frac{\delta}{4}\frac{(\rho_w - \rho_b)}{\rho} Re_b^2 \tag{20}$$

Thus, the Richardson ratio $\varphi = \frac{Ri_c}{Ri_g}$ is defined to analyze the combined effects between buoyancy and centrifugal force for supercritical hydrocarbon fuel in helical tubes. Fig. 10 shows Richardson ratio variations for different experimental conditions. It is concluded that the centrifugal force effects on heat transfer is relatively small within 10 times compared with buoyancy effect when the inlet Reynolds number is below 3000. Moreover, the Richardson number is approximately linear increase along the helical tube before the pseudo-critical temperature. When the Richardson number is about 10, the value is starting to increase exponentially due to the sharp decrease of density gradient in the radial direction. Hence, $\varphi > 10$ is proposed to judge that centrifugal force take the main lead to influence heat transfer in helical tube and buoyancy effect could be neglected.

3.3. Heat transfer correlation

The earliest researches about heat transfer characteristics are mainly on pure fluid in the straight circular tube. Jackson and Hall

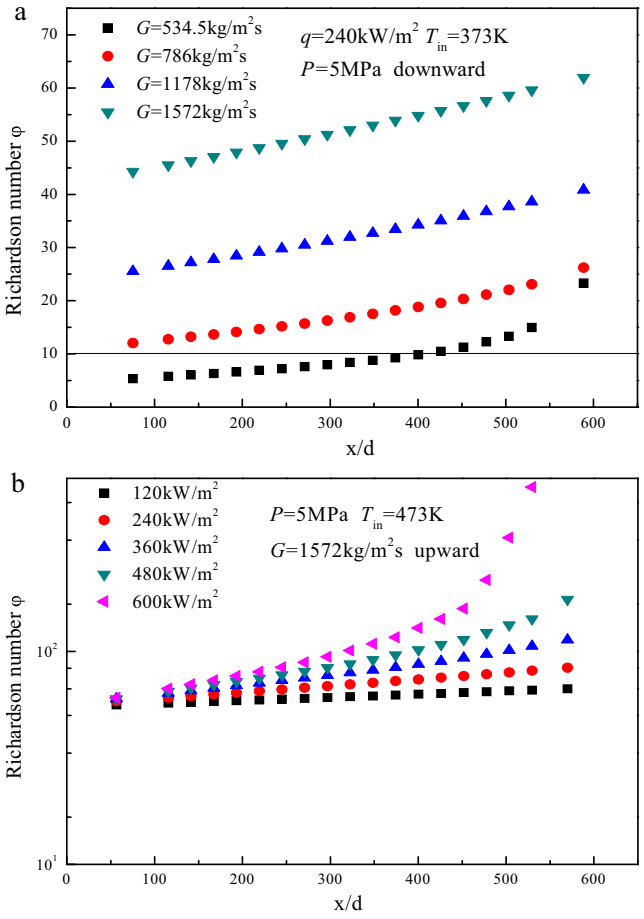

Fig. 10. Richardson ratio distributions at different working conditions.

[47] established half experience calculated formula considering buoyancy effect by theoretical analysis as follows:

$$\frac{Nu}{Nu_f} = \left[\left|1 \pm \frac{8\times 10^4 Gr^*}{Re^{3.425} Pr^{.8}}\left(\frac{Nu}{Nu_f}\right)^{-2}\right|\right]^{0.46} \tag{21}$$

"+" represents downward flow and "−"is upward flow. Nu_f is Dittus-Boelter Nusselt number which is modified correlation with thermal properties variation.

$$Nu_f = 0.0183 Re_b^{0.82} Pr_b^{0.5}\left(\frac{\overline{c_p}}{c_{pb}}\right)^n \left(\frac{\rho_w}{\rho_b}\right)^{0.3} \tag{22}$$

With the widely research in CCA technology, hydrocarbon fuel at supercritical pressures is studied more and more. One regular correlation concluded by experimental data of *n*-decane was proposed by Jiang [43] in the following equation.

$$\frac{Nu}{Nu_f} = \left[\left|1 + A\cdot Bo^*\left(\frac{\overline{c_p}}{c_{pb}}\right)^a \left(\frac{\rho}{\rho_b}\right)^b \left(\frac{Nu}{Nu_f}\right)^{-2}\right|\right]^{0.46} \tag{23}$$

where A, a and b values are different for upward and downward flows. Fig. 11a displays comparison between above two calculated values and experimental data. It is seen that Nusselt numbers predicted by two correlations exist large deviation in the wide range, especially when the $Nu > 200$. The reason is that the correlation do not consider the heat transfer enhancement by centrifugal force.

Furthermore, heat transfer characteristics in curved channel are mainly on the fluid with constant property. Xin and Ebadian [48]

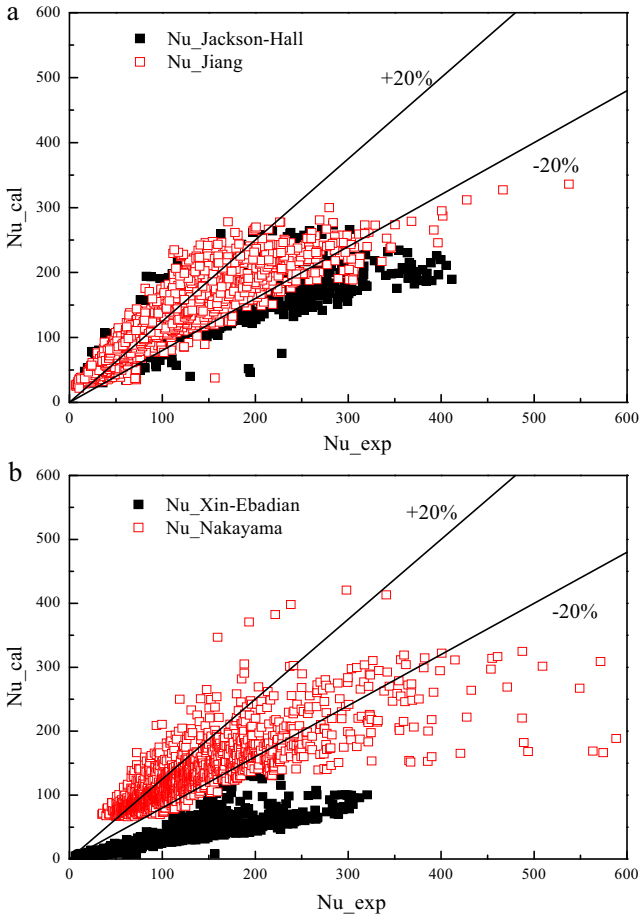

Fig. 11. Comparison between calculated Nusselt numbers of correlations and experimental data.

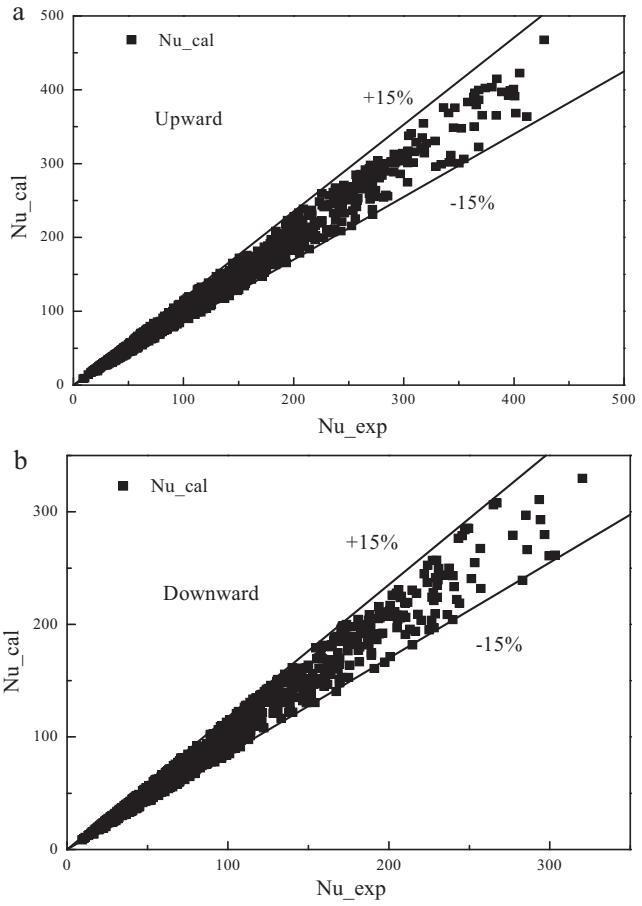

Fig. 12. Comparison between calculated Nusselt numbers of Eqs. (26) and (27) and experimental data.

put forward the following Nusselt number experimental correlation in helical tubes at low Reynolds number conditions.

$$Nu = 0.00619Re^{0.91}Pr^{0.4}\left[1 + 3.455\left(\frac{d}{R}\right)\right] \tag{24}$$

Mori and Nakayama [49] researched turbulent heat transfer variation under constant heat flux in helical tube. The results indicate that the enhancement in turbulent flow is not good as in the laminar flow and forced convection heat transfer correlation is summarized as follows.

$$Nu_c = \frac{1}{41}\left\{1 + \frac{0.061}{\left[Re(d/R)^{2.5}\right]^{1/6}}\right\} \cdot Re^{5/6} \cdot (d/R)^{1/12} \cdot Pr^{0.4} \tag{25}$$

Fig. 11b shows Nusselt number comparison between correlation values and experimental data. Xin-Ebadian correlation predicted value totally smaller than experimental data with the reason that experimental helical tube has small bending diameter. For the Nakayama correlation, the predicted value exists large divergence in the high Nusselt number range. The reason is that the Nakayama correlation could not consider density and viscosity variations at the near wall at supercritical pressures.

According to the above analysis, centrifugal force takes the key lead to influence convective heat transfer distribution and buoyancy has obvious influence at some specific conditions. Thus, all experimental data are summarized to obtain two correlations for forced convection of hydrocarbon fuel in helical tube heated at supercritical pressure considering Richardson ratio φ.

$$\text{Upward flow}: \frac{Nu}{Nu_f} = 0.0524 \cdot \varphi^{0.016} \cdot \left(\frac{\rho_w}{\rho_b}\right)^{0.548}\left(\frac{\mu_w}{\mu_b}\right)^{0.292}\left[1 + 21.3\left(\frac{Nu}{Nu_f}\right)^{1.035}\right] \tag{26}$$

$$\text{Downward flow}: \frac{Nu}{Nu_f} = 0.0541 \cdot \varphi^{0.016} \cdot \left(\frac{\rho_w}{\rho_b}\right)^{0.548}\left(\frac{\mu_w}{\mu_b}\right)^{0.292}\left[1 + 20.2\left(\frac{Nu}{Nu_f}\right)^{1.05}\right] \tag{27}$$

where Nu_f is defined as follows:

$$Nu_f = 0.0113Re^{0.862}Pr_f^{0.4} \tag{28}$$

Fig. 12 shows the comparison between experimental data and calculated value. 99.7% of 1446 data point for upward flow and 95.7% of downward flow data are within the ±15% error band.

4. Conclusion

Convective heat transfer characteristics of aviation kerosene RP-3 flowing in a vertical helical tube at supercritical pressure were experimentally investigated in this paper. Considering combined effects between buoyancy and centrifugal force, the following conclusions were obtained.

(1) Nusselt number increases slowly along the helical tube and values are much smaller than that in the turbulent flow. The turbulent mixing could enhance twice larger in HTC with centrifugal force effect.
(2) The secondary flow induced by centrifugal force move outward of the cross section and the outside HTC is averagely 31.5% larger than the inside.
(3) $Bo^* > 2 \times 10^{-7}$ could not predict buoyancy effect on heat transfer in helical tube. Centrifugal secondary flow turns into the key factor to produce heat transfer enhancement when the Richardson ratio $\varphi > 10$.
(4) Two correlations of Nusselt number are developed to predict convective heat transfer of aviation kerosene RP-3 at supercritical pressure in the vertical helical tube.

Acknowledgement

The authors would like to acknowledge the financial support provided by the China National Natural Science Foundation (Grant No. 51606179).

References

[1] W. Dean, J. Hurst, Note on the motion of fluid in a curved pipe, Mathematika 6 (01) (1959) 77–85.
[2] G. Yang, Z. Dong, M. Ebadian, Laminar forced convection in a helicoidal pipe with finite pitch, Int. J. Heat Mass Transf. 38 (5) (1995) 853–862.
[3] R.C. Xin, M.A. Ebadian, Natural convection heat transfer from helicoidal pipes, J. Thermophys. Heat Transf. 10 (2) (1996) 297–302.
[4] C. Lin, M. Ebadian, Developing turbulent convective heat transfer in helical pipes, Int. J. Heat Mass Transf. 40 (16) (1997) 3861–3873.
[5] C. Lin, M. Ebadian, The effects of inlet turbulence on the development of fluid flow and heat transfer in a helically coiled pipe, Int. J. Heat Mass Transf. 42 (4) (1999) 739–751.
[6] D. Prabhanjan, G. Raghavan, T. Rennie, Comparison of heat transfer rates between a straight tube heat exchanger and a helically coiled heat exchanger, Int. Commun. Heat Mass 29 (2) (2002) 185–191.
[7] P. Coronel, K. Sandeep, Heat transfer coefficient in helical heat exchangers under turbulent flow conditions, Int. J. Food Eng. 4 (1) (2008).
[8] J.S. Jayakumar, S.M. Mahajani, J.C. Mandal, K.N. Iyer, P.K. Vijayan, CFD analysis of single-phase flows inside helically coiled tubes, Comput. Chem. Eng. 34 (4) (2010) 430–446.
[9] L. Janssen, C. Hoogendoorn, Laminar convective heat transfer in helical coiled tubes, Int. J. Heat Mass Transf. 21 (9) (1978) 1197–1206.
[10] C. Yildiz, Y. Biçer, D. Pehlivan, Heat transfers and pressure drops in rotating helical pipes, Appl. Energy 50 (1) (1995) 85–94.
[11] C. Yildiz, Y. Biçer, D. Pehlivan, Heat transfer and pressure drop in a heat exchanger with a helical pipe containing inside springs, Energy Convers. Manage. 38 (6) (1997) 619–624.
[12] D. Austen, H. Soliman, Laminar flow and heat transfer in helically coiled tubes with substantial pitch, Exp. Therm. Fluid Sci. 1 (2) (1988) 183–194.
[13] B. Prasad, D. Das, A. Prabhakar, Pressure drop, heat transfer and performance of a helically coiled tubular exchanger, Heat Recov. Syst. CHP 9 (3) (1989) 249–256.
[14] L. Guo, X. Chen, Z. Feng, B. Bai, Transient convective heat transfer in a helical coiled tube with pulsatile fully developed turbulent flow, Int. J. Heat Mass Transf. 41 (19) (1998) 2867–2875.
[15] K.A. Misurati, Y. Quan, W. Gong, G. Xu, Y. Yan, Contrastive study of flow and heat transfer characteristics in a helically coiled tube under uniform heating and one-side heating, App. Therm. Eng. 114 (2017) 77–84.
[16] G. Bruening, W. Chang, Cooled cooling air systems for turbine thermal management, ASME Paper, (99-GT), 1999, pp. 14.
[17] W. Hall, Heat transfer near the critical point, Adv. Heat Transf. 7 (1971) 1–86.
[18] J. Jackson, W. Hall, Forced convection heat transfer to fluids at supercritical pressure, Turbul. Forced Convect. Channels Bund. 2 (1979) 563–611.
[19] J.D. Jackson, Fluid flow and convective heat transfer to fluids at supercritical pressure, Nucl. Eng. Des. 264 (2013) 24–40.
[20] P.-X. Jiang, Y. Zhang, Y.-J. Xu, R.-F. Shi, Experimental and numerical investigation of convection heat transfer of CO_2 at supercritical pressures in a vertical tube at low Reynolds numbers, Int. J. Therm. Sci. 47 (8) (2008) 998–1011.
[21] P.-X. Jiang, B. Liu, C.-R. Zhao, F. Luo, Convection heat transfer of supercritical pressure carbon dioxide in a vertical micro tube from transition to turbulent flow regime, Int. J. Heat Mass Transf. 56 (1) (2013) 741–749.
[22] J.R. Krieger, L.-D. Chen, Measurements of heat transfer to near-critical fluids, in: AIAA/ASME/SAE/ASEE Joint Propulsion Conference & Exhibit, 33rd, Seattle, WA, 1997.
[23] P.A. Masters, C. Aukerman, Deposit formation in hydrocarbon rocket fuels with an evaluation of a propane heat transfer correlation, AIAA Paper 1290 (1982).
[24] E. Krasnoshchekov, V. Protopopov, Experimental study of heat exchange in carbon dioxide in the supercritical range at high temperature drops (heat transfer in turbulent carbon dioxide pipeflow at supercritical region), High Temp. 4 (1966) 375–382.
[25] B. Stiegemeier, M. Meyer, R. Taghavi, A thermal stability and heat transfer investigation of five hydrocarbon fuels, in: 38th AIAA/ASME/SAE/ASEE Joint Propulsion Conference & Exhibit, AIAA, 2002, pp. 1–10.
[26] H. Deng, C. Zhang, G. Xu, Z. Tao, K. Zhu, Y. Wang, Visualization experiments of a specific fuel flow through quartz-glass tubes under both sub- and supercritical conditions, Chin. J. Aeronaut. 25 (3) (2012) 372–380.
[27] H. Deng, K. Zhu, G. Xu, Z. Tao, C. Zhang, G. Liu, Isobaric specific heat capacity measurement for kerosene RP-3 in the near-critical and supercritical regions, J. Chem. Eng. Data 57 (2) (2011) 263–268.
[28] H. Deng, C. Zhang, G. Xu, Z. Tao, B. Zhang, G. Liu, Density measurements of endothermic hydrocarbon fuel at sub-and supercritical conditions, J. Chem. Eng. Data 56 (6) (2011) 2980–2986.
[29] H. Deng, C. Zhang, G. Xu, B. Zhang, Z. Tao, K. Zhu, Viscosity measurements of endothermic hydrocarbon fuel from (298 to 788) K under supercritical pressure conditions, J. Chem. Eng. Data 57 (2) (2012) 358–365.
[30] H. Deng, K. Zhu, G. Xu, Z. Tao, J. Sun, Heat transfer characteristics of RP-3 kerosene at supercritical pressure in a vertical circular tube, J. Enhanc. Heat Transf. 19 (5) (2012).
[31] C. Zhang, G. Xu, L. Gao, Z. Tao, H. Deng, K. Zhu, Experimental investigation on heat transfer of a specific fuel (RP-3) flows through downward tubes at supercritical pressure, J. Supercrit. Fluid 72 (2012) 90–99.
[32] K. Zhu, G.-Q. Xu, Z. Tao, H.-W. Deng, Z.-H. Ran, C.-B. Zhang, Flow frictional resistance characteristics of kerosene RP-3 in horizontal circular tube at supercritical pressure, Exp. Therm. Fluid Sci. 44 (2013) 245–252.
[33] W. Li, D. Huang, G.-Q. Xu, Z. Tao, Z. Wu, H.-T. Zhu, Heat transfer to aviation kerosene flowing upward in smooth tubes at supercritical pressures, Int. J. Heat Mass Transf. 85 (2015) 1084–1094.
[34] D. Huang, X.-Y. Wu, Z. Wu, W. Li, H.-T. Zhu, B. Sunden, Experimental study on heat transfer of nanofluids in a vertical tube at supercritical pressures, Int. Commun. Heat Mass 63 (2015) 54–61.
[35] D. Huang, Z. Wu, B. Sunden, W. Li, A brief review on convection heat transfer of fluids at supercritical pressures in tubes and the recent progress, Appl. Energy 162 (2016) 494–505.
[36] D. Huang, B. Ruan, X. Wu, W. Zhang, G. Xu, Z. Tao, P. Jiang, L. Ma, W. Li, Experimental study on heat transfer of aviation kerosene in a vertical upward tube at supercritical pressures, Chin. J. Chem. Eng. 23 (2) (2015) 425–434.
[37] Y. Fu, J. Wen, Z. Tao, G. Xu, H. Huang, Experimental research on convective heat transfer of supercritical hydrocarbon fuel flowing through U-turn tubes, Appl. Therm. Eng. 116 (2017) 43–55.
[38] C. Zhang, H. Deng, G. Xu, W. Huang, K. Zhu, Enthalpy measurement and heat transfer investigation of RP-3 kerosene at supercritical pressure, J. Aerosp. Power 25 (2) (2010) 331–335.
[39] G. Xu, Z. Jia, J. Wen, H. Deng, Y. Fu, Thermal-conductivity measurements of aviation kerosene RP-3 from (285 to 513) K at sub-and supercritical pressures, Int. J. Thermophys. 36 (4) (2015) 620–632.
[40] H. Ito, Friction factors for turbulent flow in curved pipes, J. Basic Eng. 81 (2) (1959) 123–134.
[41] P. Srinivasan, S. Nandapurkar, F. Holland, Friction factors for coils, Trans. Inst. Chem. Eng. 48 (1970) T156–T161.
[42] E.F. Schmidt, Wärmeübergang und druckverlust in rohrschlangen, Chem. Ing. Tech. 39 (13) (1967) 781–789.
[43] B. Liu, Y. Zhu, J.-J. Yan, Y. Lei, B. Zhang, P.-X. Jiang, Experimental investigation of convection heat transfer of n-decane at supercritical pressures in small vertical tubes, Int. J. Heat Mass Transf. 91 (2015) 734–746.
[44] B. Morton, Laminar convection in uniformly heated horizontal pipes at low Rayleigh numbers, Quart. J. Mech. Appl. Math. 12 (4) (1959) 410–420.
[45] C. Wang, On the low-Reynolds-number flow in a helical pipe, J. Fluid Mech. 108 (1981) 185–194.
[46] M. Ciofalo, A. Arini, M. Di Liberto, On the influence of gravitational and centrifugal buoyancy on laminar flow and heat transfer in curved pipes and coils, Int. J. Heat Mass Transf. 82 (2015) 123–134.
[47] J. Jackson, M. Cotton, B. Axcell, Studies of mixed convection in vertical tubes, Int. J. Hat Fluid Flow 10 (1) (1989) 2–15.
[48] R.C. Xin, M. Ebadian, The effects of Prandtl numbers on local and average convective heat transfer characteristics in helical pipes, J. Heat Trans. – T ASME 119 (3) (1997) 467–473.
[49] Y. Mori, W. Nakayama, Study of forced convective heat transfer in curved pipes (2nd report, turbulent region), Int. J. Heat Mass Transf. 10 (1) (1967) 37–59.